Photoinduced topological phase transition from a crossing-line nodal semimetal to a multiple-Weyl semimetal

Motohiko Ezawa

Phys. Rev. B **96**, 041205 — Published 21 July 2017

DOI: 10.1103/PhysRevB.96.041205

Photoinduced topological phase transition from a crossing-line nodal semimetal to a multiple-Weyl semimetal

Motohiko Ezawa
Department of Applied Physics, University of Tokyo, Hongo 7-3-1, 113-8656, Japan

We propose a simple scheme to construct a model whose Fermi surface is comprised of crossing-line nodes. The Hamiltonian consists of a normal hopping term and an additional term which is odd under the mirror reflection. The line nodes appear along the mirror-invariant planes, where each line node carries the quantized Berry magnetic flux. We explicitly construct a model with the N-fold rotational symmetry, where the $2N$ line nodes merge at the north and south poles. When we apply photoirradiation along the k_z axis, there emerge point nodes carrying the monopole charge $\pm N$ at these poles, while all the line nodes disappear. In this model, photoirradiation induces a topological phase transition from a crossing-line nodal semimetal to a multiple-Weyl semimetal, where the surface state turns from a drum-head state into a Fermi-arc state.

Introduction: Weyl semimetal is one of the hottest topics in condensed matter physics[1,2]. It is protected by a monopole charge in the momentum space[3]. Multiple Weyl semimetal is a generalization of a Weyl semimetal which has a monopole charge larger than the unit charge[4,5,7,56]. There exist another class of novel semimetals. They are line nodal semimetals whose Fermi surfaces form one-dimensional lines[8–25]. A line node is protected by a quantized Berry magnetic flux. Recently, line nodal semimetals are generalized into two species. One is a loop node forming a nontrivial link such as the Hopf link[26–29]. The other is a crossing-line node, where several line nodes cross at a point[30–35].

Photoirradiation is a powerful tool to modify the band structure[36–41]. According to the Floquet theory an additional term emerges due to the second-order process of photoirradiation. A typical example is the generation of a Weyl point from a Dirac semimetal[42–44,46]. A Weyl node can also be generated by applying photoirradiation to a loop nodal semimetal[45–49].

In this paper, we first propose a simple scheme to construct models for crossing-line nodal semimetals. We then investigate how a crossing-line nodal semimetal is modified by way of photoirradiation. The model Hamiltonian consists of a normal hopping term and a mirror-odd interaction term. A line node emerges on the mirror-invariant plane. Each line node is topologically protected by the quantized Berry magnetic flux. Explicitly, we construct an N-fold rotational symmetric model, where the crossing of $2N$-fold line nodes occurs at the north pole and also at the south pole. There are no magnetic monopoles at these poles. Next, we derive a photoinduced term based on the Floquet theory. It induces a topological phase transition. Indeed, by applying photoirradiation along the z direction, the Fermi surface is found to disappear by the emergence of gap except for two nodal points carrying the N ($-N$) units of the monopole charge at the north (south) pole. The resultant system is the anisotropic N-fold multiple-Weyl semimetal.

Model: A prototype of line nodal semimetals is given by the model

$$H(\mathbf{k}) = f_x(\mathbf{k})\sigma_x + f_z(\mathbf{k})\sigma_z, \tag{1}$$

whose energy spectrum reads $E(\mathbf{k}) = \pm\sqrt{f_x^2(\mathbf{k}) + f_z^2(\mathbf{k})}$. The Fermi surface is given by the two conditions $f_x(\mathbf{k}) = 0$ and $f_z(\mathbf{k}) = 0$, each of which produces a two-dimensional surface. The intersection of the two surfaces consists of lines and/or points, generating line nodes and/or point nodes, in general. For simplicity we consider the following cases: (i) The condition $f_x(\mathbf{k}) = 0$ generates an ellipsoid, which is rotational symmetric around the k_z axis and centered at the origin ($\mathbf{k} = 0$). (ii) The condition $f_x(\mathbf{k}) = 0$ generates planes sharing the k_z axis with each other. Furthermore we require that $f_z(\mathbf{k})$ is odd under the mirror operation M_α with respect to each plane, where the index α denotes the direction normal to the plane. For example, if $f_z(\mathbf{k})$ is odd for the mirror reflection with respect to the k_yk_z plane, $M_x f_z(k_x,k_y,k_z)M_x^{-1} = -f_z(-k_x,k_y,k_z)$, we have a zero-energy solution at $k_x = 0$ since $M_x f_z(0,k_y,k_z)M_x^{-1} = -f_z(0,k_y,k_z)$.

A key observation is that, when there are N mirror-odd planes, there emerges the crossing of $2N$ line nodes. For example, by assuming the N-fold rotation symmetry, the lattice Hamiltonian is given by (1) together with

$$f_x(\mathbf{k}) = t\sum_{j=1}^{N}\cos\left(\mathbf{d}_j^c\cdot\mathbf{k}\right) + t_z\cos k_z - m',$$
$$f_z(\mathbf{k}) = \lambda' g\left(k_z\right)\prod_{j=1}^{N}\sin\left(\mathbf{d}_j^s\cdot\mathbf{k}\right), \tag{2}$$

where $\mathbf{d}_j^c = \left(\cos\left[j\pi/N\right],\sin\left[j\pi/N\right],0\right)$ and $\mathbf{d}_j^s = d_N\left(\sin\left[\left(2j+1\right)\pi/\left(2N\right)\right],\cos\left[\left(2j+1\right)\pi/\left(2N\right)\right],0\right)$, where $d_1 = d_3 = 1$ and $d_2 = \sqrt{2}$. We have included a function $g\left(k_z\right)$ to allow the freedom of introducing additional crossing-line modes perpendicular to the k_z axis such as in (14) for the cubic symmetric model. The summation $\sum_{j=1}$ runs over the nearest neighbor sites. The Fermi surface is given by the cross section of the N planes and the ellipsoid. They are $2N$ line nodes which cross at the north and south poles. We show Fermi surfaces for $N = 2$ and $N = 3$ in Figs.1(a1) and (c1), respectively. (Actually, we present almost zero-energy surfaces $E = \delta$ with $0 < \delta \ll t$.) We note that the lattice structure is possible in the real space only for $N = 2$ and 3. The lattice with $N = 2$ forms a layered square lattice, while the lattice with $N = 3$ forms a layered triangular lattice. Nevertheless, we analyze the general N case to make the mathematical structure clearer. See Supplemental Material[50] on the lattice structure described by the model (1) together with (2).

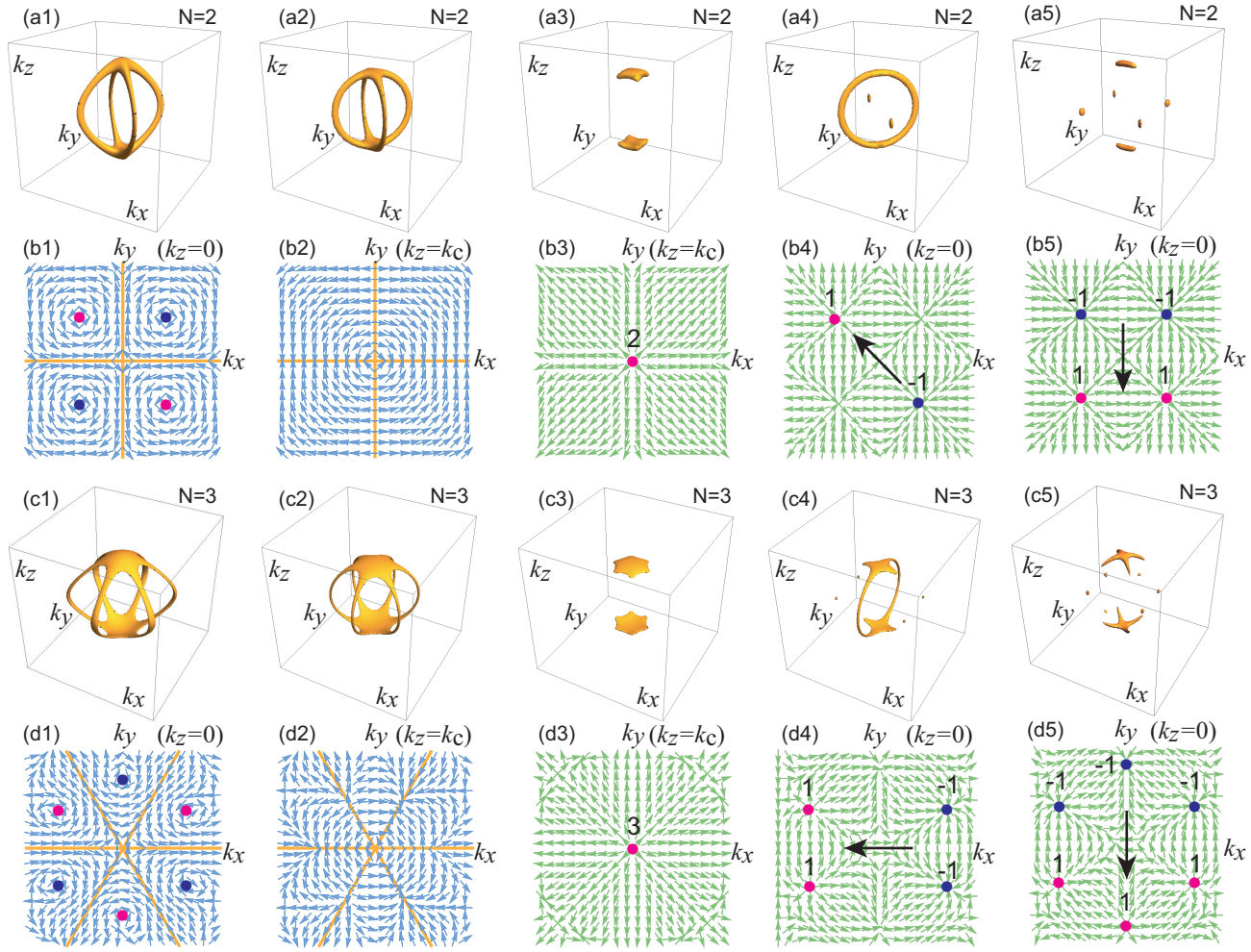

FIG. 1: Bird's-eye of the almost zero-energy surfaces of the Hamiltonian with $N = 2$ for (a1) the lattice model, (a2) the continuum model, (a3) the continuum model with photoirradiation along the k_z axis, (a4)–(d5) the continuum model with photoirradiation perpendicular to the k_z axis, where the direction is indicated by arrows as in (b4)–(b5). (b1) Normalized Berry connection $(A_x, A_y)/\sqrt{A_x^2 + A_y^2}$ for the lattice model with $N = 2$ on the $k_z = 0$ plane. Red (blue) dots represent vortices and antivortices. The total vorticity is zero. (b2) Normalized Berry connection for $N = 2$ on the $k_z = k_c$ plane, where the north pole is present at the center of the plane. There are no vortices and no monopoles there. (b3) Normalized Berry curvature $(B_x, B_y)/\sqrt{B_x^2 + B_y^2}$ corresponding to (a3) on the $k_z = k_c$ plane. (b4)–(b5) Normalized Berry curvature corresponding to (a4)–(a5) on the $k_z = 0$ plane. Red (blue) dots represent monopoles and antimonopoles carrying the monopole charges indicated by the attached numbers. No monopoles appear at the north and south poles. (c1)–(c5) The corresponding bird's eye's view for $N = 3$. (d1)–(d2) The corresponding normalized Berry connection for $N = 3$. (d3)–(d5) The corresponding normalized Berry curvature for $N = 3$, where the direction of the photoirradiation is indicated by arrows.

The corresponding continuum theory is given by

$$H = [a\left(k_x^2 + k_y^2\right) + ck_z^2 - m]\sigma_x + \lambda g\left(k_z\right) \mathrm{Re}(k_+^N)\sigma_z \quad (3)$$

with $a = -Nt/4$, $c = -t_z/2$, $m = m' + Nt + t_z$ and $\lambda = \lambda'/2^{N-1}$. For example, for the case of $N = 2$, there are two mirror planes M_{x+y} and M_{x-y}. A simplest representation is $f_z = k_x^2 - k_y^2$, whose zero-energy solution is given by the two planes $k_x = k_y$ and $k_y = -k_y$. For the case of $N = 3$, there are three mirror planes determined by $f_z = k_x^3 - 3k_x k_y^2$. We show the Fermi surfaces in Figs.1(a2) and (b2). The Fermi surfaces obtained in the continuum theory are found to be almost the same as those obtained in the lattice model. Hence, we use the continuum theory in the following.

With the use of the eigenfunction $|\psi\rangle$ of the Hamiltonian (3) we may calculate the Berry connection as $A_i\left(\mathbf{k}\right) = -i\left\langle\psi\right|\partial_i\left|\psi\right\rangle = \frac{1}{2}\partial_i\Theta$ with $\partial_i = \partial/\partial k_i$, where $f_x = f\cos\Theta$, $f_z = f\sin\Theta$ and $f = \sqrt{f_x^2 + f_z^2}$. We show the stream plot of the Berry connection for $N = 2$ and 3, where vortex and antivortex structures are observed around the line nodes in the constant k_z plane, as in Figs.1(b1) and (d1). A pair of vortex and antivortex is annihilated at the north and south poles as in Figs.1(b2) and (d2). Each line node is topologically protected since the Berry phase along the line node is quantized as $\oint A_j dk_j = \int \nabla \times \mathbf{A}\, dS = \pm\pi$. The Berry curvature $\mathbf{B} = \nabla \times \mathbf{A}$ is strictly localized along the line node. Indeed,

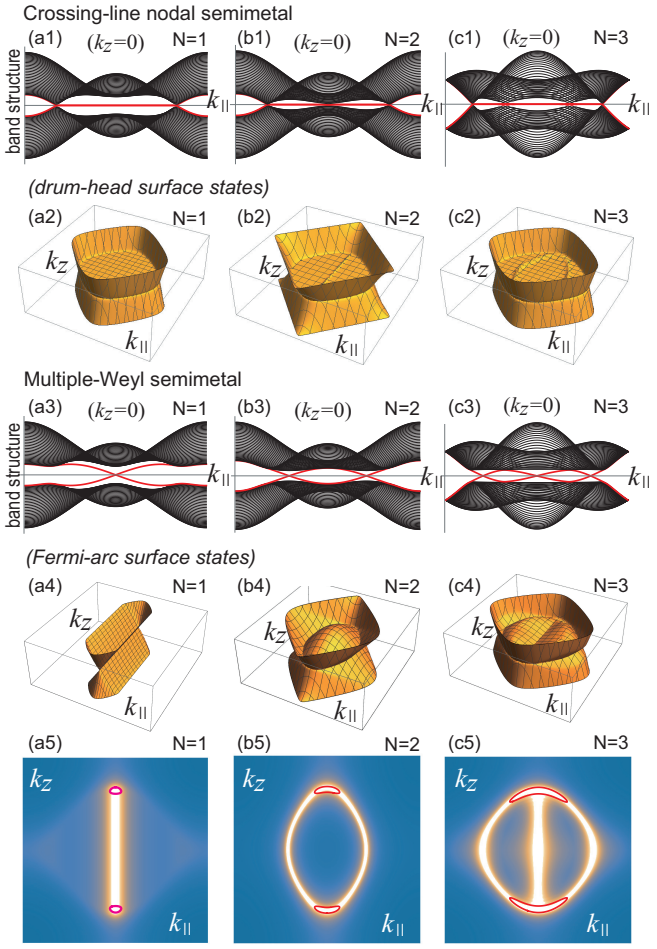

FIG. 2: Thin-film band structures of a crossing-line nodal semimetal with (a1) $N = 1$, (b1) $N = 2$, and (c1) $N = 3$, where the surface states are emphasized by red color. We have set $k_z = 0$. (a2)–(c2) They are called drum-head surface states. Thin-film band structure of a multiple-Weyl semimetal with (a3) $N = 1$, (b3) $N = 2$, and (c3) $N = 3$, where the surface states are emphasized by red color. (a4)–(c4) They are called Fermi-arc surface states. (a5)–(c5) Fermi arcs connecting the north and south poles for them. Almost-zero energy states ($E = \delta$ with $|\delta| \ll 1$) of the bulk spectrum are shown in red curves.

we can explicitly check this by the direct calculation,

$$B_i(\mathbf{k}) = \varepsilon_{ijk}\partial_j A_k = \pm\pi \sum \delta(f_x)\,\delta(f_y)\,. \tag{4}$$

The Berry magnetic flux is present along each line node, while the Berry curvature is strictly zero away from the line nodes. Consequently a line node is topologically protected.

Photoirradiation parallel to the k_z axis: We proceed to investigate a topological phase transition due to the σ_y term induced by photoirradiation. The following formulas hold for any function $g(k_z)$ in (2). First, we irradiate a beam of circularly polarized light along the z direction. We take the electromagnetic potential as $\mathbf{A}_{\rm EM}(t) = (A\cos\omega t, A\sin\omega t, 0)$, where ω is the frequency of light with $\omega > 0$ for the right circulation and $\omega < 0$ for the left circulation. The effective Hamiltonian is the sum of the $2n$-th order photoirradiation process, and is given by[36–41]

$$\Delta H_{\rm eff}(\mathbf{k},\mathbf{A}) = \frac{1}{\hbar\omega}\sum_{n\geq 1}\frac{[H_{-n}(\mathbf{k},\mathbf{A}_{\rm EM}), H_{+n}(\mathbf{k},\mathbf{A}_{\rm EM})]}{n}, \tag{5}$$

with $H_{\pm n}(\mathbf{k},\mathbf{A}) = \frac{1}{T}\int_0^T H(\mathbf{k}+e\mathbf{A})\,e^{\pm in\omega t}dt$. It is explicitly calculated as $\Delta H_{\rm eff}(\mathbf{k},\mathbf{A}_{\rm EM}) = f_y\sigma_y$, where $f_y = -2na\lambda\alpha g(k_z){\rm Im}(k_+^N)$ with $\alpha = (eA)^2/(\hbar\omega)$. This is the second order term ($n = 1$), while all higher order terms ($n \geq 2$) are zero. The total effective Hamiltonian is

$$H(\mathbf{k}) = f_x(\mathbf{k})\sigma_x + f_y(\mathbf{k})\sigma_y + f_z(\mathbf{k})\sigma_z, \tag{6}$$

with the energy $E(\mathbf{k}) = \pm\sqrt{f_x^2(\mathbf{k}) + f_y^2(\mathbf{k}) + f_z^2(\mathbf{k})}$. Now the zero-energy conditions become $f_x(\mathbf{k}) = f_y(\mathbf{k}) = f_z(\mathbf{k}) = 0$. In general, there is no intersection between three surfaces, and the system becomes an insulator. However, there are several cases where crossing-line nodes are reduced to points nodes, as shown in Figs.1(a3) and (c3).

The Fermi surface consists of only two point nodes at the north and south poles, $(k_x, k_y, k_z) = (0, 0, k_{\rm c})$ with $k_{\rm c} = \pm\sqrt{m/c}$. In the vicinity of these points, we obtain $f_z \approx \pm 2\sqrt{mc}\left(k_z \mp \sqrt{m/c}\right)$. The Hamiltonian with photoirradiation is given by

$$H = \pm 2\sqrt{mc}\left(k_z \mp \sqrt{m/c}\right)\sigma_x + \lambda g(k_z)\,{\rm Re}(k_+^N)\sigma_z - 2na\lambda\alpha g(k_z)\,{\rm Im}(k_+^N)\sigma_y. \tag{7}$$

In particular, when $2na(eA)^2 = \hbar\omega$ and $g(k_z) = 1$, the Hamiltonian is reduced to that of the multiple-Weyl fermion,

$$H = \lambda\left(k_+^N\sigma_+ + k_-^N\sigma_-\right) \pm 2\sqrt{mc}\left(k_z \mp \sqrt{m/c}\right)\sigma_z, \tag{8}$$

and otherwise it is reduced to that of the anisotropic multiple-Weyl fermion. The Berry curvature is calculated as $F_i(\mathbf{k}) = \varepsilon_{ijk}(\partial_j\mathbf{f}\times\partial_k\mathbf{f})\cdot\mathbf{f}$, where $\mathbf{f} = (f_x, f_y, f_z)$ with $f_x = f\cos\Phi\sin\Theta$, $f_y = f\sin\Phi\sin\Theta$, $f_z = f\cos\Theta$. It describes monopoles with the charges $\pm N$ at the north and south poles. We illustrate the Berry curvature around the north pole for $N = 2$ and 3 in Figs.1(b3) and (d3) for the case of $g(k_z) = 1$, where the presence of the monopoles is observed as a source or a sink of the Berry magnetic flux. We conclude that, by applying photoirradiation along the z direction, the Fermi surface changes from the nodal crossing lines to the two nodal points carrying the N ($-N$) units of the monopole charge at the north (south) pole. Namely, a topological phase transition has occurred from a crossing-line nodal semimetal to a multiple-Weyl semimetal.

We show the band structures of a crossing-line nodal semimetal and a multiple-Weyl semimetal along the $k_\parallel$ axis at $k_z = 0$ in Figs.2(a1)–(c1) and (a3)–(c3), respectively, where $k_\parallel = k_y$ for $N = 1$ and $N = 3$, while $k_\parallel = k_x + k_y$ for $N = 2$. The drum-head surface states, which are characterized by partial-flat band inside the projected line nodes, appear and connect the line nodes with the opposite Berry flux in Figs.2(a2)–(c2). These drum-head surface states turn

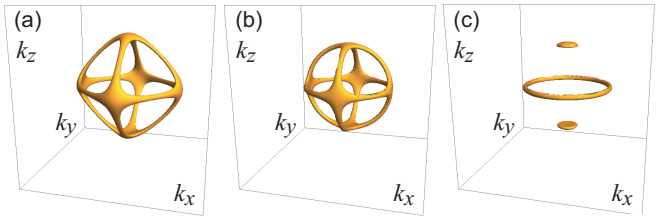

FIG. 3: Bird's-eye view of the almost zero-energy surfaces of the Hamiltonian with the cubic symmetry for (a) the lattice model, (b) the continuum model, (c) the continuum model with photoirradiation along the k_z axis. Each loop node carries the unit Berry magnetic flux in (a)–(c). The point nodes at the north and south poles carry the ± 2 units of Berry monopole charges.

into N-Fermi arcs once the system turns into a multiple-Weyl semimetal by photoirradiation. Fermi arcs are observed in Figs.2(a4)–(c4) and (a5)–(c5).

Photoirradiation perpendicular to the k_z axis: We next apply photoirradiation perpendicular to the k_z axis. We explicitly study the tetragonal symmetric model ($N = 2$) and the trigonal symmetric model ($N = 3$). We set $g(k_z) = 1$ in (2).

The lattice Hamiltonian of the tetragonal symmetric model with $N = 2$ is given by

$$\begin{aligned} f_x &= t\left(\cos k_x + \cos k_y\right) + t_z \cos k_z - m', \\ f_z &= -\lambda\left(\cos k_x - \cos k_y\right). \end{aligned} \tag{9}$$

We inject photoirradiation along the ϕ direction with $\mathbf{A}_{\rm EM}(t) = (-A\sin\phi\cos\omega t, A\cos\phi\cos\omega t, A\sin\omega t)$. The induced term is given in the continuum theory by

$$f_y = -\alpha\lambda t_z k_z\left(k_x\sin\phi + k_y\cos\phi\right). \tag{10}$$

Solving $f_x = f_z = f_y = 0$, we obtain the Fermi surface.

When $\phi = \pi/4$ or $-\pi/4$, there emerge a loop node along the $k_x = k_y$ plane or the $k_x = -k_y$ plane, and two zero-energy points emerge at the two points $(k_x, k_y, k_z) = (\pm k_c, \pm k_c, 0)$ or $(\pm k_c, \mp k_c, 0)$ with $k_c = \sqrt{m/2t}$. By expanding the Hamiltonian around these points the dispersion relation is found to be linear. For instance, at $\phi = \pi/4$ it reads

$$H = \pm k_c\left(tk_y''\sigma_x - 2\alpha k_z\sigma_y - 2\lambda k_x''\sigma_z\right) \tag{11}$$

with $k_x'' = k_x' + k_y'$, $k_y'' = k_x' - k_y'$, $k_x' = k_x \mp k_c$, $k_y' = k_x \pm k_c$. Hence, they are Weyl point nodes carrying the unit monopole charge: See Figs.1(a4) and (b4). Unless $\phi = \pm\pi/4$, only Weyl point nodes appear as in Figs.1(a5) and (b5).

The lattice Hamiltonian of the trigonal symmetric model with $N = 3$ is given by

$$\begin{aligned} f_x &= t\left(\cos k_x + \sum_{\eta=\pm 1}\cos\frac{-k_x + \eta\sqrt{3}k_y}{2}\right) + t_z\cos k_z - m, \\ f_z &= \frac{\lambda}{2}\sin k_x\left(\cos k_x - \cos\sqrt{3}k_y\right). \end{aligned} \tag{12}$$

The photoinduced term reads in the continuum theory as

$$f_y = \alpha\frac{3\lambda t_z}{4}k_z\left(\left(k_x^2 - k_y^2\right)\sin\phi + 2k_xk_y\cos\phi\right). \tag{13}$$

When $\phi = \pi/2, \pi/2 \pm 2\pi/3$, a loop node and four point nodes emerge as in Figs.1(c4) and (d4), and otherwise only points modes emerge. Namely, a loop node emerge only when the direction of photoirradiation is perpendicular to the loop node. Figs.1(c5) and (d5).

Cubic symmetric model: Finally, we present a simple realization of a lattice model with the cubic symmetry by taking

$$\begin{aligned} f_x &= t\left(\cos k_x + \cos k_y + \cos k_z\right) - m', \\ f_z &= \lambda'\sin k_x\sin k_y\sin k_z, \end{aligned} \tag{14}$$

where we have set $g(k_z) = \sin k_z$ in (2). We illustrate the Fermi surface of the lattice model and the continuum model in Figs.3(a) and (b). Photoirradiation applied along the z direction induces the term

$$f_y = \alpha\lambda t k_z\left(k_x^2 - k_y^2\right) \tag{15}$$

in the continuum theory. Solving $f_x = f_z = f_y = 0$, we obtain a loop mode given by $k_x^2 + k_y^2 = 2(3t - m)/t$ and $k_z = 0$. Additionally anisotropic double-Weyl points emerge at the north and south poles, carrying the monopole charge ± 2. We illustrate the Fermi surface in Fig.3(c).

Discussions: Crossing-line nodal semimetals with the cubic symmetry are realizable in CaTe and Cu_3PdN according to recent first principles calculations in Ref.[34] and Ref.[32,35], respectively. LaN has also a crossing line node[30], which is topologically identical to the cubic symmetric model. Furthermore, the hexagonal hydride, YH_3, has a crossing-line nodes with $N = 3$, for which the material parameters fitted by first-principles calculations[33] are $a = 8.314\text{eV}\text{Å}^2$, $c = 8.082\text{V}\text{Å}^2$, $m = -0.15156\text{eV}$, $\lambda = 0.70\text{eV}\text{Å}^3$ and $g(k_z) = 1$ in the Hamiltonian (3). In these materials there are no or almost no spin-orbit interactions. When spin-orbit interactions are present, the system turns into a topological or trivial insulator[33]. See Supplemental Material for details[50]. It is an interesting problem to search further materialization of crossing-line node semimetals.

We have shown that photoirradiation induces a topological phase transition from a crossing-line nodal semimetal to a multiple-Weyl semimetal. The easiest way to detect the emergence of multiple-Weyl semimetals would be to observe the anomalous Hall effect and/or the Adler-Bell-Jackiew anomaly: See Supplemental Material for more details[50]. In deriving this phase transition, to avoid the optical absorption, we need an off-resonant light to be soft X ray with 4000THz, which corresponds to the band gap 3eV. To open a gap $\Delta = 300\text{K} = 25\text{meV}$, the required intensity[37,47] is $3\times 10^{12}\text{W/cm}^2$, which gives $A = 0.09$. It is experimentally feasible[51–54].

The author is very grateful to N. Nagaosa for many helpful discussions on the subject. This work is supported by the Grants-in-Aid for Scientific Research from MEXT KAKENHI (Grant Nos.JP17K05490, 25400317 and 15H05854). This work was also supported by CREST, JST (Grant No. JPMJCR16F1).

[1] P. Hosur, X.L. Qi, C. R. Physique **14**, 857 (2013).
[2] S. Jia, S.-Y. Xu, M. Z. Hasan, Nature Materials **15**, 1140 (2016).
[3] S. Murakami, New J. Phys. 9, 356 (2007).
[4] C. Fang, M. J. Gilbert, X. Dai, and B. A. Bernevig, Phys. Rev. Lett. **108**, 266802 (2012).
[5] B.-J. Yang and N. Nagaosa, Nat. Commun. **5**, 4898 (2014).
[6] X. Li, B. Roy and S. Das Sarma, Phys. Rev. B **94**, 195144 (2016).
[7] S.-M. Huang, S.-Y. Xu, I. Belopolski, C.-C. Lee, G. Chang, T.-R. Chang, B. Wang, N. Alidoust, G. Bian, M. Neupane, D. Sanchez, H. Zheng, H.-T. Jeng, A. Bansil, T. Neupert, H. Lin, and M. Z. Hasan, Proc. Natl. Acad. Sci. **113**, 1180 (2016).
[8] A. A. Burkov, M. D. Hook, and L. Balents, Phys. Rev. B **84**, 235126 (2011).
[9] C. Fang, Y. Chen, H.-Y. Kee and L. Fu, Phys. Rev. B **92**, 081201 (2015).
[10] L. S. Xie, L. M. Schoop, E. M. Seibel, Q. D. Gibson, W. Xie, and R. J. Cava, APL Materials **3**, 083602 (2015).
[11] A. Yamakage, Y. Yamakawa, Y. Tanaka, Y. Okamoto, J. Phys. Soc. Jpn. **85**, 013708 (2016).
[12] M. Ezawa, Phys. Rev. Lett. Phys. Rev. Lett. **116**, 127202 (2016).
[13] M. Hirayama, R. Okugawa, T. Miyake, and S. Murakami, Nat. Com. **8**, 14022 (2017).
[14] Y.-H. Chan, C.-K. Chiu, M. Y. Chou, and A. P. Schnyder, Phys. Rev. B **93**, 205132 (2016).
[15] J.-M. Carter, V.V. Shankar, M. A. Zeb, and H.-Y. Kee, Phys. Rev. B **85**, 115105 (2012).
[16] M. Phillips and V. Aji, Phys. Rev. B **90**, 115111 (2014).
[17] Y. Chen, Y.-M. Lu, and H.-Y. Kee, Nat. Commun. **6**, 6593 (2015).
[18] C.-K. Chiu and A. P. Schnyder, Phys. Rev. B **90**, 205136 (2014).
[19] K. Mullen, B. Uchoa, and D. T. Glatzhofer, Phys. Rev. Lett. **115**, 026403 (2015).
[20] H. Weng, Y. Liang, Q. Xu, R. Yu, Z. Fang, X. Dai, and Y. Kawazoe, Phys. Rev. B **92**, 045108 (2015).
[21] G. Bian, T.-R. Chang, R. Sankar, S.-Y. Xu, H. Zheng, T. Neupert, C.-K. Chiu, S.-M. Huang, G. Chang, I. Belopolski, D. S. Sanchez, M. Neupane, N. Alidoust, C. Liu, B. Wang, C.-C. Lee, H-T. Jeng, C. Zhang, Z. Yuan, S. Jia, A. Bansil, F. Chou, H. Lin, and M. Z. Hasan, Nat. Commun. **7**, 10556 (2016).
[22] J.-W. Rhim and Y.B. Kim, Phys. Rev. B **92**, 045126 (2015).
[23] Y. Chen, Y. Xie, S. A. Yang, H. Pan, F. Zhang, M. L. Cohen, and S. Zhang, Nano Lett. **15**, 6974 (2015).
[24] C. Fang, Y. Chen, H.-Y. Kee, and L. Fu, Phys. Rev. B **92**, 081201 (2015).
[25] G. Bian, T.-R. Chang, H. Zheng, S. Velury, S.-Y. Xu, T. Neupert, C.-K. Chiu, S.-M. Huang, D. S. Sanchez, I. Belopolski, N. Alidoust, P.-J. Chen, G. Chang, A. Bansil, H.-T. Jeng, H. Lin, and M. Z. Hasan, Phys. Rev. B **93**, 121113 (2016).
[26] W. Chen, H.-Z. Lu, and J.-M. Hou, Phys. Rev. B **96**, 041102(R) (2017).
[27] Z. Yan, R. Bi, H. Shen, L. Lu, S.-C. Zhang, and Z. Wang, Phys. Rev. B 96, 041103(R) (2017).
[28] P.-Y. Chang and C.-H. Yee, cond-mat/arXiv:1704.01948.
[29] M. Ezawa, Phys. Rev. B **96**, 041202(R) (2017).
[30] M. Zeng, C. Fang, G. Chang, Y.-A. Chen, T. Hsieh, A. Bansil, H. Lin, and L. Fu, arXiv:1504.03492.
[31] T. Bzduek, Q.-S. Wu, A. Ruegg, M. Sigrist and A. A. Soluyanov, Nature **538**, 75 (2016).
[32] Y. Kim, B. J. Wieder, C. L. Kane, and A. M. Rappe, Phys. Rev. Lett. **115**, 036806 (2015).
[33] S. Kobayashi, Y. Yamakawa, A. Yamakage, T. Inohara, Y. Okamoto, and Y. Tanaka, Phys. Rev. B 95, 245208 (2017).
[34] Y. Du, F. Tang, D. Wang, L. Sheng, E.-j. Kan, C.-G. Duan, S. Y. Savrasov, and X. Wan, npj Quantum Materials (2017) 2:3.
[35] R. Yu, H. Weng,Z. Fang, X. Dai and X. Hu, Phys. Rev. Lett. **115**, 036807 (2015).
[36] T. Oka and H. Aoki, Phys. Rev. B **79**, 081406(R) (2009).
[37] T. Kitagawa, T. Oka, A. Brataas, L. Fu, and E. Demler, Phys. Rev. B **84**, 235108 (2011).
[38] N. Lindner, G. Refael and V. Gaslitski, Nat. Phys. **7**, 490 (2011).
[39] B. Dóra, J. Cayssol, F. Simon and R. Moessner, Phys. Rev. Lett. **108**, 056602 (2012).
[40] M. Ezawa, Phys. Rev. Lett. **110**, 026603 (2013).
[41] N. Goldman and J. Dalibard, Phys. Rev. X **4**, 031027 (2014).
[42] R. Wang, B. Wang, R. Shen, L. Sheng and D. Y. Xing, EPL **105**, 17004 (2014).
[43] C.-K. Chan, P. A. Lee, K. S. Burch, J. H. Han, and Y. Ran, Phys. Rev. Lett. **116**, 026805 (2016).
[44] S. Ebihara, K. Fukushima, and T. Oka, Phys. Rev. B **93**, 155107 (2016).
[45] Z. Yan and Z. Wang, Phys. Rev. Lett. **117**, 087402 (2016).
[46] C.-K. Chan, Y.-T. Oh, J. H. Han, and P. A. Lee, Phys. Rev. B **94**, 121106(R) (2016).
[47] A. Narayan, Phys. Rev. B **94**, 041409 (2016).
[48] K. Taguchi, D.-H. Xu, A. Yamakage, and K. T. Law, Phys. Rev. B **94**, 155206 (2016).
[49] M. Ezawa, Phys. Rev. B **95**, 205201 (2017).
[50] See Supplemental Material at [URL will be inserted by publisher] for details on the lattice structure and the tight-binding model, on the effect of the spin-orbit interaction, and also on the anomalous Hall effects and the chiral anomally as an experimental signature of the emergence of the multiple-Weyl semimetal, which includes Refs.[55,56][These references in Supplemental Material not already in paper].
[51] R. W. Schoenlein, S. Chattopadhyay, H. H. Chong, T. E. Glover, P.A. Heimann, C.V. Shank, A. A. Zholents, and M. S. Zolotorev, Science **287**, 2237 (2000).
[52] Y. Wang, H. Steinberg, P. Jarillo-Herrero, and N. Gedik, Science **342**, 453 (2013).
[53] E. J. Sie, J. W. McIver, Y.-H. Lee, L. Fu, J. Kong, and N. Gedik, Nature materials **14**, 290 (2015).
[54] J. Kim, X. Hong, C. Jin, S.-F. Shi, C.-Y. S. Chang, M.-H. Chiu, L.-J. Li, and F. Wang, Science **346**, 1205 (2014).
[55] B. Roy and J. D. Sau, Phys. Rev. B **92**, 125141 (2015).
[56] X. Li, B. Roy and S. Das Sarma, Phys. Rev. B **94**, 195144 (2016)